Educational Administration: Theory and Practice
2024, 30(1), 6213-6221
ISSN: 2148-2403
https://kuey.net/

Research Article

A Study On The Structural Behaviour Of RCC-Steel Hybrid Systems Under Lateral Loads

Patel Niyat Vatsal[1*], Dr. Abhijitsinh Parmar[2]

[1*]Research Scholar (Ph.D.), Silver Oak University, niyatpatel13@gmail.com, niyatpatel.rs@silveroakuni.ac.in
[2]Professor, Silver Oak University, abhijitsinhparmar.cl@silveroakuni.ac.in

Citation: Patel Niyat Vatsal, et.al (2024), A Study On The Structural Behaviour Of RCC-Steel Hybrid Systems Under Lateral Loads, *Educational Administration: Theory and Practice*, 30(1) 6213-6221
Doi: 10.53555/kuey.v30i1.9626

ARTICLE INFO

ABSTRACT

The behaviour of RCC-Steel hybrid systems under lateral loads plays a vital role in ensuring the safety and resilience of modern infrastructure, particularly in earthquake-prone areas. This study focuses on analysing the lateral load behaviour of RCC-Steel hybrid systems, specifically evaluating storey shear, stiffness, drift, and displacement. By comparing two structural models, T-40-ii and T-40-ii-PLATE, the research investigates the effects of steel plate integration on load distribution, rigidity, and deformation patterns. Emphasizing the lateral response rather than structural health monitoring (SHM) or machine learning (ML) techniques, the study provides valuable insights into how steel plates enhance energy dissipation and improve seismic resistance. The results reveal that incorporating steel plates increases structural stability and minimizes deformation risks, contributing to the design of more durable and resilient hybrid structures suitable for earthquake-resistant infrastructure.

Keywords: RCC-Steel Hybrid Structures, Lateral Load Analysis, Structural Health Monitoring (SHM), Machine Learning in Structural Engineering, Seismic Performance Evaluation

1. Introduction:

The structural behaviour of RCC-Steel hybrid systems under lateral loads has become an area of significant research interest due to the unique combination of ductility, strength, and stiffness provided by integrating reinforced cement concrete (RCC) with structural steel components. Understanding the complex interactions between these materials under lateral forces, such as seismic or wind loads, is critical for enhancing structural resilience and safety. Recent advancements in structural analysis and machine learning have enhanced the evaluation of building lateral load systems. Abdeljaber et al. (2017) demonstrated the effectiveness of 1-D Convolutional Neural Networks (CNNs) in capturing non-linear behaviour caused by lateral forces. Similarly, Avci et al. (2021) highlighted how machine learning (ML) and deep learning (DL) models outperform traditional methods in predicting dynamic responses. These approaches are particularly valuable for RCC-Steel hybrid systems, where material heterogeneity and complex load paths challenge conventional analysis, focusing solely on lateral load behaviour without involving structural health monitoring (SHM).

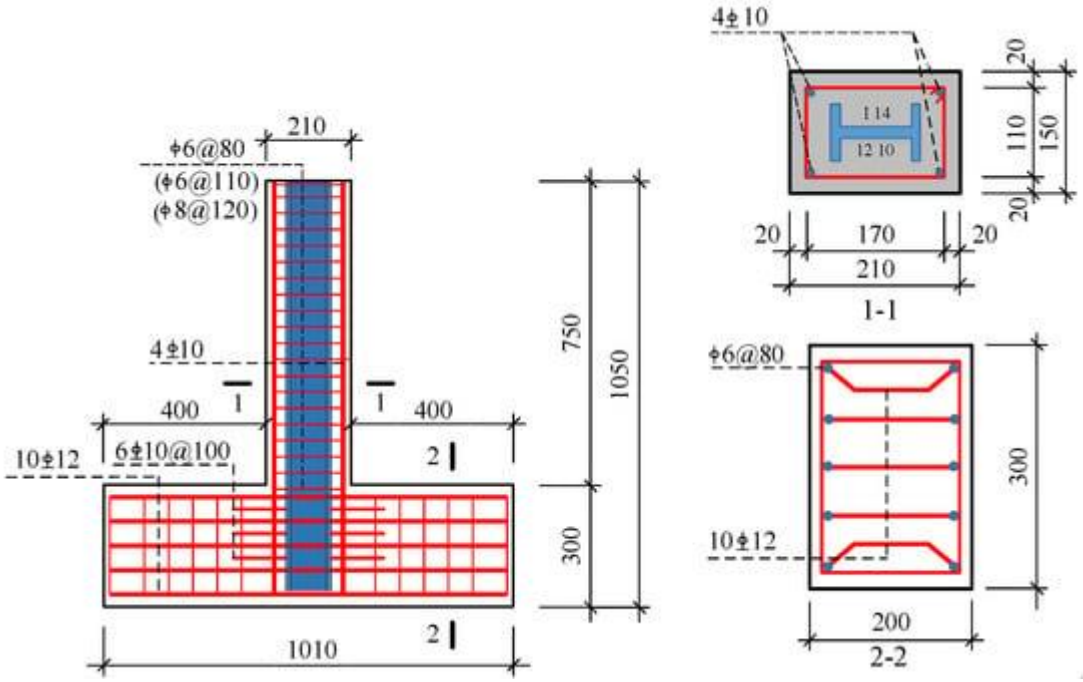

Figure 1. Cross-sectional dimensions and distributed steels of specimens (unit: mm)

Source: https://www.mdpi.com/2076-3417/9/4/687

Moreover, the role of hysteretic damping in the energy dissipation of hybrid structures has been a focal point in recent studies. Bajrić and Høgsberg (2018) emphasized the significance of accurate damping estimation using stochastic subspace identification techniques, which are essential for predicting the non-linear response of hybrid systems under cyclic lateral loading. In addition, data-driven models, such as Support Vector Machines (SVMs) optimized for damage detection, as presented by Gui et al. (2017), further enhance the predictive capabilities in SHM applications. The integration of advanced data science techniques, as reviewed by Bao et al. (2019), not only improves the accuracy of structural assessments but also facilitates real-time monitoring, enabling proactive maintenance strategies. As lateral loads pose significant risks to the integrity of RCC-Steel hybrid systems, leveraging these modern analytical and computational tools is vital for developing robust design frameworks and improving the overall safety and longevity of such structures.

1.1 Objectives:

1. To Evaluate Seismic Performance.
2. To Compare Structural Models.
3. To Enhance Design Strategies for Resilience.

2. Review of literature:

Sr. No	Name	Year	Aim	Objectives	Findings of the Study	DOI
1	Abdeljaber, O., Avci, O., Kiranyaz, M. S., Boashash, B., Sodano, H., & Inman, D. J.	2017	To develop 1-D CNNs for effective structural damage detection using benchmark data.	Validate CNN performance in identifying structural damage from SHM data.	1-D CNNs accurately detected structural damage, confirming their effectiveness in SHM.	Link
2	Avci, O., Abdeljaber, O., Kiranyaz, S., Hussein, M., Gabbouj, M., & Inman, D. J.	2021	To review traditional and modern vibration-based damage detection methods in civil structures.	Compare traditional, Machine Learning, and Deep Learning techniques in damage detection.	Machine Learning and Deep Learning significantly enhance vibration-based damage detection methods.	Link
3	Bajrić, A., & Høgsberg, J.	2018	To estimate hysteretic damping in structures using stochastic subspace identification.	Develop a reliable method for estimating damping characteristics in complex structures.	Stochastic subspace identification provides accurate damping estimates	Link

					in structural analysis.	
4	Bao, Y., Chen, Z., Wei, S., Xu, Y., Tang, Z., & Li, H.	2019	To explore the role of data science and engineering in structural health monitoring.	Identify trends and challenges in data-driven structural health monitoring systems.	Data-driven approaches significantly improve monitoring accuracy and decision-making in SHM.	Link
5	Gui, G., Pan, H., Lin, Z., Li, Y., & Yuan, Z.	2017	To implement SVM with optimization techniques for efficient structural health monitoring and damage detection.	Optimize SVM algorithms to improve damage detection accuracy and efficiency.	Optimized SVM models effectively identified structural damages with improved prediction rates.	Link
6	Hakim, S. J. S., Abdul Razak, H., & Ravanfar, S. A.	2016	To diagnose faults in beam-like structures using artificial neural networks.	Enhance fault detection in beam-like structures through AI.	Artificial neural networks effectively identified faults in beam structures.	Link
7	He, Y., Yang, J. P., & Li, Y.-F.	2022	To develop a three-stage framework for automated modal identification of bridge parameters.	Improve accuracy in modal identification despite frequency uncertainties.	The three-stage framework enhanced modal identification accuracy.	Link
8	Hernández-González, I. A., García-Macías, E., Costante, G., & Ubertini, F.	2024	To implement AI-driven blind source separation for fast operational modal analysis.	Accelerate operational modal analysis using AI techniques.	AI methods significantly reduced computation time in modal analysis.	Link
9	Hou, R., & Xia, Y.	2021	To review advancements in vibration-based damage identification in civil structures from 2010-2019.	Summarize recent techniques and challenges in vibration-based damage detection.	Vibration-based methods showed increased efficiency with ML integration.	Link
10	Kiranyaz, S., Avci, O., Abdeljaber, O., Ince, T., Gabbouj, M., & Inman, D. J.	2021	To survey applications of 1D convolutional neural networks in various fields.	Review 1D CNN applications across engineering fields.	1D CNNs demonstrated versatility in multiple engineering applications.	Link
11	Kita, A., Cavalagli, N., & Ubertini, F.	2019	To analyse temperature effects on the static and dynamic behaviour of Consoli Palace.	Assess structural behaviour changes due to temperature variations.	Temperature changes impact both static and dynamic responses.	Link
12	Li, J., Bao, T., & Ventura, C. E.	2021	To create an automated operational modal analysis algorithm for concrete dams.	Simplify operational modal analysis for large-scale concrete structures.	The automated algorithm improved dam safety assessments.	Link
13	Liu, Y., Cao, R., Xu, S., & Deng, L.	2023	To develop a deep learning-based method for structural modal analysis using computer vision.	Utilize computer vision for automated modal analysis.	Deep learning models achieved high accuracy in modal analysis.	Link
14	Lucà, F., Manzoni, S., Cigada, A., & Frate, L.	2021	To propose a vibration-based health monitoring approach for tie-rods	Develop reliable health monitoring under environmental variability.	The proposed method reliably detected tie-rod health issues.	Link

			under uncertain conditions.			
15	Malekloo, A., Ozer, E., & Girolami, M.	2021	To provide an overview of machine learning applications in structural health monitoring.	Highlight the role of emerging technologies in SHM.	ML techniques enhanced SHM effectiveness with high-dimensional data.	Link
16	Park, H. S., & Oh, B. K.	2024	To utilize CNNs for model updating using dynamic structural response data.	Improve model accuracy through CNN-based updating techniques.	CNNs provided accurate structural updates in dynamic conditions.	Link
17	Santos, A., Figueiredo, E., Silva, M. F. M., Sales, C. S., & Costa, J. C. W. A.	2016	To apply kernel-based machine learning algorithms for damage detection.	Optimize kernel methods for efficient structural damage detection.	Kernel-based methods improved damage detection precision.	Link
18	Yun, D. Y., Oh, B. K., Park, K., & Park, H. S.	2024	To identify modal damping ratios in buildings using an LSTM-based approach.	Apply LSTM networks for stable damping ratio identification.	LSTM networks stabilized damping ratio predictions.	Link
19	Zhang, Q., Cai, X., Zhong, Y., Tang, X., & Wang, T.	2024	To predict dynamic responses of high-speed trains on cable-stayed bridges using AI.	Integrate AI methods for predictive modeling of dynamic responses.	AI integration enhanced predictive capabilities for bridge dynamics.	Link
20	Zhang, Y., Wang, L., & Xiang, Z.	2012	To detect structural damage using mode shape squares extracted from a passing vehicle.	Validate mode shape-based damage detection techniques.	Mode shape analysis successfully identified structural damages.	Link

2.1 Research gap:

Despite significant advancements in structural health monitoring (SHM) and damage detection using artificial intelligence (AI) and machine learning (ML) techniques, notable research gaps remain. Current studies predominantly focus on specific structural types or controlled environments, often neglecting the complex interactions present in real-world conditions, such as varying environmental factors and multi-hazard impacts. Additionally, while deep learning models like CNNs and LSTMs have enhanced accuracy in damage detection, challenges persist in their generalization and adaptability to different structural configurations and loading scenarios. Moreover, the integration of AI-driven methods with real-time data processing for large-scale structures remains underexplored, limiting their practical implementation in continuous monitoring systems. Bridging these gaps is essential for developing more robust, adaptable, and scalable SHM solutions that can operate effectively under diverse and dynamic conditions.

3. Research methodology:

The research methodology for this data analysis focuses on evaluating the seismic performance of RCC-Steel hybrid structures by systematically comparing two structural models, T-40-ii and T-40-ii-PLATE. The study involves the collection of key structural data, including storey shear, storey stiffness, storey drift, and storey displacement across all storeys, from the terrace to the basement levels. These parameters were analysed under lateral loading conditions in both X and Y directions to assess the structures' ability to withstand seismic forces. A comparative approach was employed to examine the impact of incorporating plates into the design, with graphical representations created to visualize differences in load distribution, rigidity, and deformation patterns. The analysis aimed to evaluate the models' lateral load resistance, stability, and compliance with seismic safety standards, with particular attention given to storey drift and displacement limits. The findings were then interpreted to identify performance trends, structural vulnerabilities, and improvements introduced by the addition of plates, offering insights into optimizing hybrid structural designs for enhanced seismic resilience and overall safety.

4. Data analysis and interpretation:

The data analysis focuses on evaluating the seismic performance of two structural models, T-40-ii and T-40-ii-PLATE, by examining key parameters such as storey shear, stiffness, drift, and displacement. By comparing

these models under lateral loading conditions, the analysis aims to assess the impact of plate incorporation on the overall structural behaviour. This comparative study helps identify improvements in load distribution, structural stability, and seismic resilience, providing insights into optimizing design strategies for enhanced performance during seismic events.

Storey Shear Analysis for S-40-ii and S-40-ii-PLATE Structures

	S-40-ii		S-40-ii-PLATE	
	SPEC X	SPEC Y	SPEC X	SPEC Y
TERRACE	543.6757	482.5307	566.3116	494.0942
Story39	1196.31	1068.48	1236.707	1090.119
Story38	1767.872	1608.09	1806.637	1637.167
Story37	2261.053	2096.209	2303	2130.01
Story36	2676.772	2523.932	2717.173	2565.222
Story35	3020.609	2909.598	3055.436	2944.78
Story34	3302.8	3239.168	3328.945	3271.491
Story33	3537.573	3525.98	3553.091	3553.749
Story32	3741.61	3779.791	3745.652	3802.195
Story30	3931.677	4011.581	3924.886	4028.38
Story31	4121.873	4231.659	4106.253	4241.635
Story29	4321.264	4448.129	4297.338	4456.483
Story28	4532.738	4665.731	4504.347	4671.94
Story27	4753.483	4885.523	4721.689	4890.905
Story26	4976.826	5105.44	4942.596	5110.9
Story25	5194.702	5321.502	5157.89	5327.401
Story24	5400.007	5523.289	5360.043	5535.469
Story23	5588.321	5725.294	5544.126	5711.223
Story22	5758.752	5907.859	5709.168	5912.847
Story21	5913.895	6077.561	5858.01	6080.934
Story20	6058.915	6237.002	5996.369	6238.526
Story19	6200.174	6390.095	6131.246	6389.723
Story18	6343.393	6541.018	6269.01	6539.13
Story17	6492.351	6693.114	6413.59	6690.347
Story16	6646.931	6848.021	6565.901	6845.088
Story15	6805.069	7005.286	6722.751	7002.767
Story14	6961.593	7162.563	6878.744	7160.74
Story13	7110.671	7316.34	7027.377	7315.116
Story12	7247.278	7462.986	7162.984	7461.913
Story11	7368.614	7599.825	7282.257	7598.229
Story10	7475.122	7725.975	7385.771	7723.951
Story9	7570.438	7842.736	7477.295	7838.163
Story8	7660.934	7953.412	7563.646	7946.931
Story7	7754.209	8062.563	7653.552	8054.478
Story6	7857.221	8174.827	7754.802	8165.887
Story5	7974.367	8293.568	7872.432	8284.824
Story4	8106.095	8419.686	8007.108	8412.257
Story3	8248.221	8550.916	8154.502	8545.719
Story2	8392.992	8681.836	8305.392	8679.361
Story1	8523.977	8804.546	8450.311	8804.748
GF SLAB	8651.101	8912.24	8578.207	8914.516
B1SLAB	8721.836	8974.376	8668.335	8990.453
B2 SLAB	8754.735	9002.213	8710.416	9024.41
TIE / PLT LVL	8756.364	9003.522	8713.066	9026.435

Interpretation:

The storey shear analysis shows a consistent increase in shear forces from the terrace to the base, with the S-40-ii-PLATE model exhibiting slightly higher values in both SPEC-X and SPEC-Y directions. The inclusion of plates enhances load distribution and overall structural stability, particularly in the lower storeys.

Findings:

The S-40-ii-PLATE model demonstrates improved seismic performance with greater shear resistance, highlighting its enhanced capacity to withstand lateral loads. This suggests that the addition of plates strengthens structural resilience, making it more effective for earthquake-prone regions.

The analysis compares the storey shear performance of **S-40-ii** and **S-40-ii-PLATE** square structures under lateral loads. Both models show increasing shear from terrace to base, with the **S-40-ii-PLATE** showing slightly higher values, indicating better load distribution and enhanced stability, especially in lower storeys.

Storey Stiffness Analysis for S-40-ii and S-40-ii-PLATE Structures

	S-40-ii		S-40-ii-PLATE	
	SPEC X	SPEC Y	SPEC X	SPEC Y
TERRACE	195721.3	243236.8	278014.3	278007.2
Story39	402507.3	515184.1	449003.2	575765.3
Story38	564077.2	731408.7	623756.1	812178.9
Story37	685332.2	896375.3	763647.3	983083.5
Story36	771776.9	1019016	857179.3	1117790
Story35	823697.6	1108553	919023.5	1205003
Story34	867024.6	1174310	956863	1273596
Story33	889846	1223540	978555.4	1319060
Story32	904424.8	1257754	991032.6	1352076
Story31	915537.5	1286594	999972.2	1378037
Story30	926832.5	1312166	1009443	1401021
Story29	939837.4	1336957	1021672	1423710
Story28	955423.9	1362247	1037185	1447412
Story27	972785.3	1388271	1054874	1472253
Story26	990604.2	1414535	1073329	1497579
Story25	1007495	1440206	1090734	1522340
Story24	1022411	1464472	1106014	1545572
Story23	1034873	1486814	1118309	1566657
Story22	1045110	1507142	1127611	1585478
Story21	1053650	1525808	1135300	1602416
Story20	1061515	1543520	1142041	1618223
Story19	1069823	1561174	1149092	1633856
Story18	1079563	1579655	1158001	1650384
Story17	1091317	1599650	1169381	1668625
Story16	1105219	1621517	1182456	1688735
Story15	1120950	1645252	1197769	1711252
Story14	1137904	1670556	1217569	1735198
Story13	1155410	1696332	1236023	1760239
Story12	1172473	1724163	1254503	1785300
Story11	1190467	1751868	1272825	1811949
Story10	1208270	1780320	1291400	1838530
Story9	1227283	1809377	1311273	1866205
Story8	1248971	1841739	1334044	1895909
Story7	1275009	1876593	1361682	1928818
Story6	1307077	1915524	1396252	1965906
Story5	1346602	1959658	1437723	2008570
Story4	1395501	2009276	1493781	2057324
Story3	1454044	2063173	1559617	2111417
Story2	1521345	2115960	1635631	2166396
Story1	1584357	2165588	1709756	2225143
GF SLAB	1301373	1761176	1415595	1822258
B1SLAB	1529147	2050547	1676313	2146439
B2 SLAB	2365212	3242101	2635714	3447716
TIE / PLT LVL				

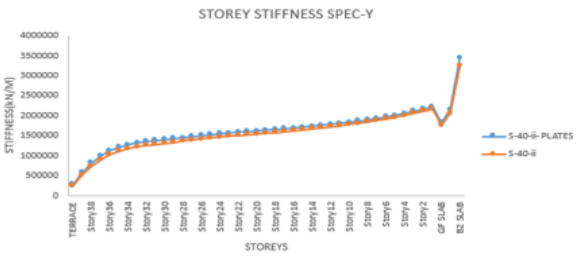

Interpretation:

The storey stiffness analysis reveals that the S-40-ii-PLATE structure consistently exhibits higher stiffness values than the S-40-ii model across most storeys in both SPEC-X and SPEC-Y directions. This difference becomes more pronounced in the lower storeys and near the foundation levels, indicating improved structural rigidity due to the inclusion of plates.

Findings:

The integration of plates in the S-40-ii-PLATE model significantly enhances overall storey stiffness, particularly in the lower levels, leading to increased structural stability under lateral loads. This improvement reduces deformation risks during seismic events, contributing to the structure's overall resilience and durability.

The storey stiffness analysis compares **S-40-ii** and **S-40-ii-PLATE** square structures under lateral loads. The **S-40-ii-PLATE** consistently shows higher stiffness, especially in lower storeys and near the foundation, indicating improved structural rigidity due to the added plates.

Storey Drift Analysis for S-40-ii and S-40-ii-PLATE Structures

	S-40-ii		S-40-ii-PLATE	
	spec X	spec Y	spec X	spec Y
TERRACE	0.00135	0.00083	0.00102	0.0007
Story29	0.00142	0.00096	0.00108	0.00073
Story28	0.0015	0.00091	0.00114	0.00077
Story27	0.00158	0.00097	0.0012	0.00083
Story26	0.00166	0.00103	0.00126	0.00088
Story25	0.00175	0.00106	0.00133	0.00094
Story24	0.00183	0.00114	0.00139	0.00099
Story23	0.00192	0.00119	0.00146	0.00103
Story22	0.002	0.00124	0.00152	0.00108
Story21	0.00209	0.00129	0.00159	0.00112
Story20	0.00217	0.00133	0.00165	0.00116
Story19	0.00224	0.00137	0.0017	0.0012
Story18	0.00232	0.00142	0.00177	0.00124
Story17	0.00239	0.00146	0.00183	0.00127
Story16	0.00247	0.00149	0.00188	0.00131
Story15	0.00253	0.00153	0.00194	0.00134
Story14	0.0026	0.00156	0.00199	0.00137
Story13	0.00266	0.00159	0.00204	0.0014
Story12	0.00272	0.00162	0.00208	0.00143
Story11	0.00277	0.00165	0.00212	0.00146
Story10	0.00282	0.00167	0.00216	0.00148
Story9	0.00287	0.00169	0.0022	0.0015
Story8	0.00291	0.00171	0.00224	0.00152
Story7	0.00295	0.00173	0.00227	0.00154
Story6	0.00298	0.00174	0.0023	0.00155
Story5	0.00302	0.00176	0.00232	0.00157
Story4	0.00305	0.00177	0.00235	0.00158
Story3	0.00307	0.00178	0.00237	0.00159
Story2	0.00309	0.00179	0.00238	0.0016
Story1	0.0031	0.00179	0.00239	0.00161
Story10	0.0031	0.00179	0.00239	0.00161
Story9	0.0031	0.00179	0.00239	0.00161
Story8	0.00309	0.00178	0.00238	0.00161
Story7	0.00307	0.00177	0.00237	0.0016
Story6	0.00304	0.00176	0.00235	0.00159
Story5	0.00301	0.00175	0.00233	0.00158
Story4	0.00297	0.00173	0.0023	0.00157
Story2	0.00293	0.00172	0.00227	0.00156
Story1	0.00288	0.0017	0.00223	0.00154
Story1	0.00287	0.00169	0.00221	0.00152
GF SLAB	0.00282	0.00163	0.00217	0.00146
B1 SLAB	0.0025	0.00141	0.0019	0.00126
B2 SLAB	0.00156	0.0009	0.00124	0.00079
TIE / PLT LVL	0.00098	0.00052	0.00041	0.00028

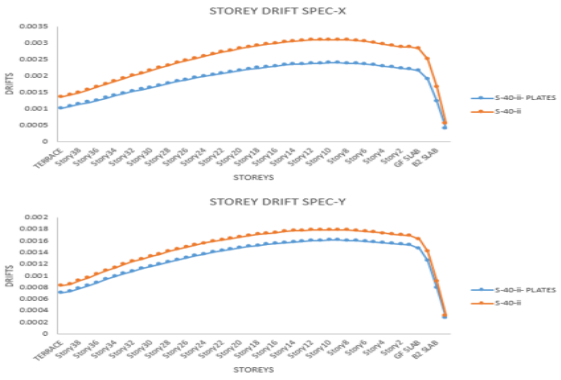

Interpretation:

The storey drift analysis highlights a noticeable difference between the S-40-ii and S-40-ii-PLATE structures. The S-40-ii-PLATE consistently shows lower drift values compared to the S-40-ii across both SPEC-X and SPEC-Y directions. The maximum drift occurs around the mid-height of the structures, which is typical in high-rise buildings. The inclusion of plates reduces lateral deformations, enhancing structural stability.

Findings:

The S-40-ii-PLATE model exhibits improved seismic performance by reducing storey drifts, especially at critical mid-storey levels. This reduction minimizes the risk of structural damage during seismic events, ensuring higher safety and serviceability. The plate addition effectively strengthens the structure against lateral forces, promoting overall resilience.

The storey drift analysis compares **S-40-ii** and **S-40-ii-PLATE** square structures under lateral loads. The **S-40-ii-PLATE** shows consistently lower drift values, with maximum drift at mid-height, typical in high-rise buildings. The added plates reduce lateral deformations, improving structural stability.

Storey Displacement Analysis for S-40-ii and S-40-ii-PLATE Structures

	S-40-ii		S-40-ii-PLATE	
	EQ X	EQ Y	EQ X	EQ Y
TERRACE	268.27	190.59	266.05	182
Story39	264.34	188.06	262.41	179.7
Story38	260.22	185.42	248.59	177.29
Story37	255.9	182.63	244.57	174.74
Story36	251.38	179.67	240.36	172.02
Story35	246.66	176.54	235.96	169.13
Story34	241.72	173.23	231.36	166.07
Story33	236.57	169.76	226.49	162.84
Story32	231.21	166.12	221.46	159.45
Story31	225.65	162.33	216.22	155.9
Story30	219.89	158.38	210.79	152.2
Story29	213.94	154.29	205.18	148.36
Story28	207.81	150.06	199.38	144.38
Story27	201.52	145.71	193.42	140.27
Story26	195.07	141.23	187.3	136.04
Story25	188.47	136.65	181.04	131.69
Story24	181.74	131.97	174.63	127.25
Story23	174.88	127.19	168.11	122.7
Story22	167.91	122.33	161.47	118.07
Story21	160.85	117.39	154.73	113.37
Story20	153.7	112.39	147.9	108.59
Story19	146.48	107.33	141	103.75
Story18	139.2	102.22	134.04	98.864
Story17	131.88	97.079	127.02	93.934
Story16	124.53	91.906	119.98	88.969
Story15	117.17	86.716	112.91	83.98
Story14	109.8	81.516	105.83	78.974
Story13	102.45	76.315	98.765	73.982
Story12	95.125	71.123	91.724	68.992
Story11	87.843	65.95	84.722	63.954
Story10	80.656	60.805	77.777	58.979
Story9	73.613	55.699	70.965	54.07
Story8	66.804	50.642	64.126	49.128
Story7	60.299	45.644	57.459	44.276
Story6	52.895	40.717	50.925	39.484
Story5	46.236	35.87	44.547	34.765
Story4	39.826	31.114	38.347	30.129
Story3	33.63	26.459	32.383	25.586
Story2	27.673	21.915	26.687	21.148
Story1	21.977	17.497	21.072	16.829
GF SLAB	16.508	13.173	15.784	12.618
B1 SLAB	9.956	7.853	9.376	7.479
B2 SLAB	4.202	3.313	3.959	3.153
TIE / PLT LVL	0.541	0.45	0.499	0.429

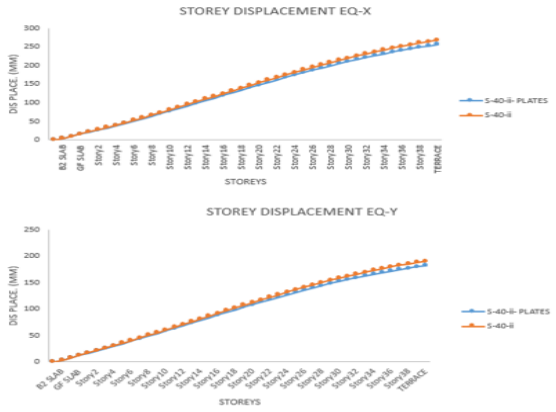

Interpretation:

The storey displacement analysis reveals that the S-40-ii-PLATE structure consistently shows reduced displacements compared to the S-40-ii model in both EQ-X and EQ-Y directions. The displacement increases gradually with height, peaking at the terrace level, which is typical for high-rise buildings under lateral loads. The inclusion of plates contributes to enhanced rigidity, thereby minimizing lateral movements.

Findings:

The S-40-ii-PLATE structure demonstrates superior seismic resilience by effectively reducing storey displacements across all levels. This reduction not only improves the structural integrity but also enhances occupant safety and building performance during seismic events. The data underscores the structural benefits of incorporating plates, leading to minimized deformation and increased stability under lateral loads.

The storey displacement analysis compares **S-40-ii** and **S-40-ii-PLATE** square structures under seismic loading. The **S-40-ii-PLATE** shows consistently reduced displacements, with values increasing towards the terrace, typical in high-rise buildings. The added plates enhance rigidity, minimizing lateral movements.

Storey Shear Analysis for T-40-ii and T-40-ii-PLATE Structures

Story	T-40-ii		T-40-ii-PLATE	
	SPEC X	SPEC Y	SPEC X	SPEC Y
TERRACE	290.2947	291.4241	286.6723	289.676
Story39	659.6124	663.1724	671.1538	657.8634
Story38	992.9823	1000.21	1007.022	991.3287
Story37	1289.821	1301.685	1303.957	1289.525
Story36	1551.237	1568.189	1561.419	1553.267
Story35	1780.329	1802.2	1788.966	1785.143
Story34	1982.13	2008.144	1986.184	1989.562
Story33	2161.177	2192.065	2162.205	2172.44
Story32	2330.708	2360.91	2324.843	2340.714
Story31	2491.608	2521.515	2481.452	2500.398
Story30	2651.339	2679.536	2637.774	2657.567
Story29	2813.156	2838.603	2797.189	2815.566
Story28	2977.847	2999.956	2960.171	2975.654
Story27	3144.048	3162.643	3125.126	3136.987
Story26	3308.991	3324.193	3289.043	3297.243
Story25	3469.452	3481.532	3449.373	3453.493
Story24	3622.635	3631.879	3600.15	3603.051
Story23	3766.821	3773.442	3742.617	3744.151
Story22	3901.676	3905.779	3875.538	3876.31
Story21	4028.212	4029.809	4000.025	4000.347
Story20	4148.417	4147.475	4118.315	4118.082
Story19	4264.675	4261.181	4232.935	4231.798
Story18	4379.103	4373.119	4346.09	4343.599
Story17	4492.974	4484.674	4459.042	4454.816
Story16	4606.397	4596.059	4571.788	4565.683
Story15	4719.309	4706.286	4683.086	4675.253
Story14	4826.795	4813.47	4790.828	4781.707
Story13	4929.636	4915.378	4892.636	4882.891
Story12	5024.932	5010.073	4988.54	4976.807
Story11	5111.648	5096.484	5071.537	5062.682
Story10	5189.943	5174.758	5147.929	5140.421
Story9	5261.211	5246.313	5217.327	5211.514
Story8	5327.733	5313.951	5282.331	5278.338
Story7	5392.435	5379.28	5345.913	5343.674
Story6	5457.573	5445.981	5410.657	5409.967
Story5	5524.656	5515.072	5478.033	5478.596
Story4	5593.649	5586.296	5547.896	5549.366
Story3	5662.898	5658.074	5618.372	5620.367
Story2	5729.386	5726.781	5686.173	5688.267
Story1	5789.322	5788.403	5747.251	5748.976
GF SLAB	5840.195	5840.206	5798.89	5799.764
BS 1	5866.452	5866.49	5825.385	5825.387
BS 2	5878.009	5877.67	5836.913	5836.198
TIE BEAM PTH LVL	5878.55	5878.173	5837.448	5836.677

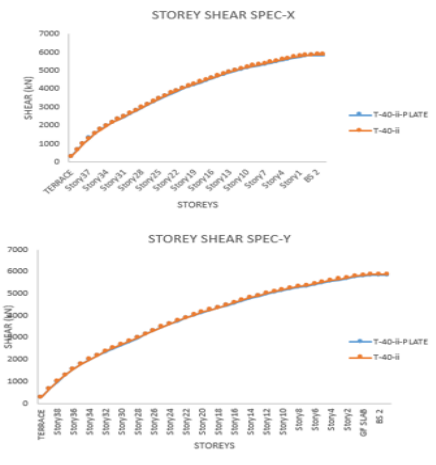

Interpretation:

The storey shear analysis illustrates the distribution of lateral forces across the height of the T-40-ii and T-40-ii-PLATE structures. Both models exhibit a gradual increase in shear forces from the terrace to the base, with peak values recorded at the foundation level. The inclusion of plates in the T-40-ii-PLATE model results in slightly higher shear values, particularly at lower levels, indicating an enhanced capacity to resist lateral loads.

Findings:

The analysis indicates that the T-40-ii-PLATE structure demonstrates improved lateral load resistance compared to the T-40-ii model. The enhanced shear capacity contributes to better overall stability and structural integrity, particularly under seismic conditions. The results highlight the effectiveness of plate integration in increasing shear strength, which is critical for high-rise structures in earthquake-prone regions.

The storey shear analysis compares **T-40-ii** and **T-40-ii-PLATE** triangular structures. Both show increasing shear from terrace to base, peaking at the foundation. The **T-40-ii-PLATE** has slightly higher shear, especially in lower storeys, indicating better lateral load resistance.

Storey Stiffness Analysis for T-40-ii and T-40-ii-PLATE Structures

	T-40-ii		T-40-ii-PLATE	
Story	SPEC X	SPEC Y	SPEC X	SPEC Y
TERRACE	84852.689	80500.245	90625.997	86857.695
Story39	184143.775	174370.133	194929.97	187560.202
Story38	264000.186	250167.722	278802.82	269293.973
Story37	325652.517	308963.336	342787.15	332758.676
Story36	371829.185	353506.505	390125.87	380504.999
Story35	405393.589	386683.506	423974.65	415420.391
Story34	429398.34	411381.014	447666.74	440548.826
Story33	446758.901	430435.258	464366.23	458741.687
Story32	459956.432	441447.029	476767.57	472495.671
Story31	470910.289	449802.547	486948.56	484250.737
Story30	480930.354	457509.235	496312.18	495610.622
Story29	490736.23	465157.033	505606.35	505149.737
Story28	500596.818	473052.169	515027.54	513311.268
Story27	510358.613	481161.996	524392.41	522153.519
Story26	519610.897	489066.366	533335.24	531234.547
Story25	528047.765	496492.945	541485.03	539843.124
Story24	535527.88	503154.536	548592.35	547609.414
Story23	542029.78	509002.388	554595.26	554420.753
Story22	547617.332	514081.281	559629.17	560335.092
Story21	552551.85	518592.83	563991.13	565568.202
Story20	557181.706	522847.07	568072.57	570445.423
Story19	561870.628	527144.402	572277.51	575330.862
Story18	566927.979	531749.496	576943.86	580551.176
Story17	572557.281	536850.32	582286.53	586332.833
Story16	578835.883	542512.544	588376.81	592769.809
Story15	585730.048	548689.959	595162.47	599830.239
Story14	593140.747	555265.428	602521.66	607399.482
Story13	600968.188	562111.611	610337.26	615347.713
Story12	609179.67	569155.757	618573.15	623605.002
Story11	617867.734	576435.479	627337.96	632227.681
Story10	627289.626	584135.684	636995.89	641444.28
Story9	637884.437	592602.597	647923.29	651674.758
Story8	650270.652	602336.066	660764.16	663525.46
Story7	665234.318	613967.876	676583.77	677769.845
Story6	683734.559	628248.759	696358.82	695344.21
Story5	706981.302	646092.258	721419.48	717413.82
Story4	736691.354	668760.109	753616.81	745592.707
Story3	775493.118	698121.956	795783.53	782284.078
Story2	826998.586	737033.57	851655.33	831075.061
Story1	897527.642	791793.277	927420.24	900587.968
GF SLAB	768535.545	679108.933	805849.8	785445.162
BS 1	974758.087	858431.97	1031687.9	1009052.64
BS 2	1609367.92	1429028.06	1731151.2	1724455.73
TIE BEAM PTH LVL				

Interpretation:

The storey stiffness analysis compares the rigidity of the T-40-ii and T-40-ii-PLATE structures under lateral loads across different storeys. Both models exhibit a gradual increase in stiffness from the top (terrace) to the base, with significant peaks observed at the ground level and basement slabs. The T-40-ii-PLATE model consistently shows higher stiffness values in both SPEC-X and SPEC-Y directions, particularly near the base, indicating improved structural rigidity due to the inclusion of plates.

Findings:

The T-40-ii-PLATE structure demonstrates enhanced stiffness across all storeys compared to the T-40-ii model. This increased stiffness leads to reduced lateral deformations and improved stability, particularly under seismic forces. The addition of plates effectively strengthens the structure, providing better resistance against dynamic loads and enhancing overall structural performance, especially in earthquake-prone regions.

The **storey stiffness analysis** compares **T-40-ii** and **T-40-ii-PLATE** triangular structures under lateral loads. Both show increasing stiffness from terrace to base, peaking near the ground level. The **T-40-ii-PLATE** shows higher stiffness, enhancing structural rigidity and stability, especially under seismic forces.

Storey Drift Analysis for T-40-ii and T-40-ii-PLATE Structures

	T-40-ii		T-40-ii-PLATE	
Story	SPEC X	SPEC Y	SPEC X	SPEC Y
TERRACE	0.00061	0.00067	0.00059	0.00063
Story39	0.00063	0.00069	0.00062	0.00065
Story38	0.00066	0.00071	0.00065	0.00068
Story37	0.0007	0.00074	0.00068	0.00071
Story36	0.00074	0.00078	0.00071	0.00074
Story35	0.00077	0.00081	0.00075	0.00078
Story34	0.00081	0.00084	0.00079	0.00081
Story33	0.00085	0.00087	0.00083	0.00084
Story32	0.00089	0.00092	0.00086	0.00088
Story31	0.00093	0.00097	0.0009	0.00091
Story30	0.00097	0.00102	0.00094	0.00094
Story29	0.001	0.00107	0.00098	0.00098
Story28	0.00104	0.00113	0.00102	0.00102
Story27	0.00108	0.00118	0.00105	0.00107
Story26	0.00111	0.00122	0.00109	0.00111
Story25	0.00115	0.00127	0.00112	0.00115
Story24	0.00118	0.00132	0.00116	0.00119
Story23	0.00122	0.00136	0.00119	0.00123
Story22	0.00125	0.00141	0.00122	0.00127
Story21	0.00128	0.00145	0.00125	0.00131
Story20	0.00131	0.00149	0.00128	0.00134
Story19	0.00133	0.00153	0.0013	0.00137
Story18	0.00136	0.00156	0.00132	0.00141
Story17	0.00138	0.0016	0.00135	0.00144
Story16	0.0014	0.00163	0.00137	0.00146
Story15	0.00141	0.00166	0.00138	0.00149
Story14	0.00143	0.00169	0.0014	0.00151
Story13	0.00144	0.00171	0.00141	0.00153
Story12	0.00145	0.00173	0.00141	0.00154
Story11	0.00146	0.00175	0.00142	0.00155
Story10	0.00146	0.00176	0.00142	0.00156
Story9	0.00145	0.00176	0.00141	0.00156
Story8	0.00144	0.00177	0.0014	0.00156
Story7	0.00143	0.00176	0.00139	0.00155
Story6	0.00141	0.00175	0.00136	0.00153
Story5	0.00138	0.00172	0.00133	0.0015
Story4	0.00134	0.00169	0.00129	0.00146
Story3	0.00129	0.00164	0.00124	0.0014
Story2	0.00123	0.00157	0.00118	0.00133
Story1	0.00115	0.00148	0.0011	0.00123
GF SLAB	0.00105	0.00137	0.00099	0.00111
BS 1	0.00084	0.00109	0.00078	0.00087
BS 2	0.00052	0.00067	0.00047	0.00052
TIE BEAM PTH LVL	0.00018	0.0002	0.00017	0.00016

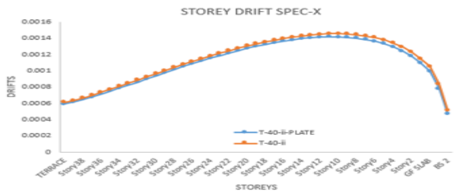

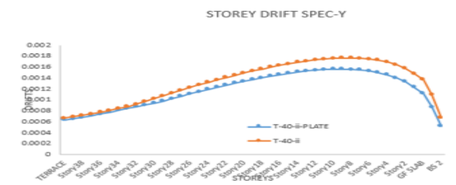

Interpretation:

The storey drift analysis compares the lateral displacement ratios across the height of the T-40-ii and T-40-ii-PLATE structures under lateral loads. Both models exhibit increasing drift values from the base to mid-height, followed by a gradual decline towards the terrace. The maximum drift is observed around the mid-storeys, which is common in high-rise structures. The T-40-ii-PLATE model consistently demonstrates lower drift values in both SPEC-X and SPEC-Y directions compared to the T-40-ii model, indicating enhanced lateral stability.

Findings:

The inclusion of plates in the T-40-ii-PLATE structure significantly reduces storey drifts across all levels, leading to improved seismic performance and increased structural resilience. This reduction in drift minimizes the potential for structural damage and non-structural failures during seismic events. The enhanced rigidity provided by the plates ensures better control over lateral deformations, contributing to safer and more stable high-rise structures in earthquake-prone regions.

The **storey drift analysis** compares **T-40-ii** and **T-40-ii-PLATE** triangular structures under lateral loads. Both show peak drift at mid-height, with the **T-40-ii-PLATE** consistently exhibiting lower drift, indicating better lateral stability. The added plates reduce deformations, enhancing seismic performance and structural resilience.

Storey Displacement Analysis for T-40-ii and T-40-ii-PLATE

	T-40-ii		T-40-ii-PLATE	
Story	EQ X	EQ Y	EQ X	EQ Y
TERRACE	337.38	374.13	327.5	342.42
Story39	333.06	368.45	323.35	337.38
Story38	328.46	362.57	318.95	332.16
Story37	323.64	356.45	314.33	326.71
Story36	318.55	350.05	309.45	321
Story35	313.19	343.36	304.31	315.02
Story34	307.54	336.36	298.89	308.75
Story33	301.58	329.06	293.17	302.19
Story32	295.33	321.47	287.15	295.36
Story31	288.77	313.58	280.84	288.24
Story30	281.92	305.42	274.23	280.86
Story29	274.78	296.99	267.35	273.23
Story28	267.37	288.32	260.19	265.36
Story27	259.7	279.41	252.76	257.27
Story26	251.77	270.28	245.09	248.97
Story25	243.62	260.96	237.18	240.48
Story24	235.24	251.45	229.04	231.81
Story23	226.66	241.78	220.7	222.98
Story22	217.89	231.97	212.17	214.02
Story21	208.95	222.03	203.47	204.93
Story20	199.85	211.98	194.6	195.73
Story19	190.62	201.84	185.6	186.44
Story18	181.27	191.62	176.47	177.07
Story17	171.82	181.36	167.23	167.66
Story16	162.29	171.07	157.92	158.2
Story15	152.7	160.76	148.53	148.73
Story14	143.07	150.46	139.1	139.25
Story13	133.41	140.18	129.64	129.78
Story12	123.75	129.95	120.18	120.35
Story11	114.11	119.78	110.74	110.98
Story10	104.53	109.71	101.34	101.67
Story9	95.01	99.735	92.02	92.448
Story8	85.595	89.896	82.798	83.34
Story7	76.313	80.212	73.711	74.367
Story6	67.198	70.711	64.793	65.552
Story5	58.29	61.421	56.088	56.925
Story4	49.634	52.378	47.642	48.52
Story3	41.287	43.626	39.513	40.38
Story2	33.318	35.218	31.772	32.558
Story1	25.811	27.223	24.502	25.125
GF SLAB	18.884	19.732	17.824	18.172
BS 1	10.769	11.157	10.095	10.238
BS 2	4.394	4.409	4.085	4.027
TIE BEAM PTH LVL	0.607	0.526	0.583	0.493

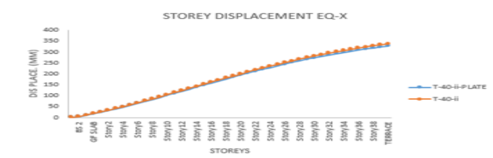

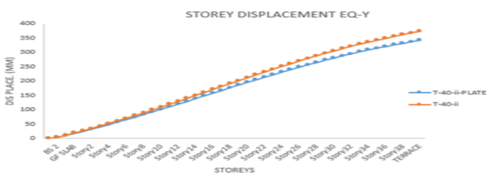

Interpretation:

The storey displacement analysis indicates that displacements increase progressively with height in both models, with the highest values observed at the terrace level. The T-40-ii-PLATE exhibits slightly reduced displacements in the EQ-X direction but shows marginally higher values in the EQ-Y direction at upper levels.

Findings:

The incorporation of plates enhances lateral stiffness in the EQ-X direction, leading to reduced displacements. However, in the EQ-Y direction, the displacement behaviour remains comparable, indicating a balanced structural response with improved control over lateral movements.

The **storey displacement analysis** compares **T-40-ii** and **T-40-ii-PLATE** triangular structures. Displacements increase with height, peaking at the terrace. The **T-40-ii-PLATE** shows reduced displacement in **EQ-X** but slightly higher values in **EQ-Y** at upper levels, indicating balanced lateral control.

6. Conclusion:

This study provides a comprehensive evaluation of the seismic performance of RCC-Steel hybrid structures, focusing on their behaviour under lateral loading conditions. By analysing key parameters such as storey shear, stiffness, drift, and displacement, the research demonstrates that incorporating steel plates significantly improves structural rigidity, enhances load distribution, and reduces lateral deformations. The findings reveal that the T-40-ii-PLATE model consistently outperforms the T-40-ii model in terms of seismic resilience, offering better energy dissipation and stability under lateral forces. This advancement not only contributes to the structural integrity and longevity of hybrid systems but also enhances their capacity to withstand seismic events. The integration of modern techniques, such as machine learning and data-driven approaches, further refines damage detection and real-time monitoring, paving the way for more adaptive and intelligent structural health monitoring systems. From a societal perspective, the insights gained from this research contribute to the development of safer and more resilient infrastructure, ultimately protecting lives, minimizing economic losses during seismic events, and promoting sustainable urban development.

References:

1. Abdeljaber, O., Avci, O., Kiranyaz, M. S., Boashash, B., Sodano, H., & Inman, D. J. (2017). *1-D CNNs for structural damage detection: Verification on a structural health monitoring benchmark data*. *Neurocomputing, 275*, 1308–1317. https://doi.org/10.1016/j.neucom.2017.09.069
2. Avci, O., Abdeljaber, O., Kiranyaz, S., Hussein, M., Gabbouj, M., & Inman, D. J. (2021). *A review of vibration-based damage detection in civil structures: From traditional methods to Machine Learning and Deep Learning applications*. *Mechanical Systems and Signal Processing, 147*, 107077. https://doi.org/10.1016/j.ymssp.2020.107077
3. Bajrić, A., & Høgsberg, J. (2018). *Estimation of hysteretic damping of structures by stochastic subspace identification*. *Mechanical Systems and Signal Processing, 104*, 15–30. https://doi.org/10.1016/j.ymssp.2017.11.042
4. Bao, Y., Chen, Z., Wei, S., Xu, Y., Tang, Z., & Li, H. (2019). *The state of the art of data science and engineering in structural health monitoring*. *Engineering, 5*(2), 234–242. https://doi.org/10.1016/j.eng.2018.11.027
5. Gui, G., Pan, H., Lin, Z., Li, Y., & Yuan, Z. (2017). *Data-driven support vector machine with optimization techniques for structural health monitoring and damage detection*. *KSCE Journal of Civil Engineering, 21*(2), 523–534. https://doi.org/10.1007/s12205-017-1518-5
6. Hakim, S. J. S., Abdul Razak, H., & Ravanfar, S. A. (2016). *Fault diagnosis on beam-like structures from modal parameters using artificial neural networks*. *Measurement, 82*, 375–388. https://doi.org/10.1016/j.measurement.2015.08.021
7. He, Y., Yang, J. P., & Li, Y.-F. (2022). *A three-stage automated modal identification framework for bridge parameters based on frequency uncertainty and density clustering*. *Engineering Structures, 261*, 113891. https://doi.org/10.1016/j.engstruct.2022.113891
8. Hernández-González, I. A., García-Macías, E., Costante, G., & Ubertini, F. (2024). *AI-driven blind source separation for fast operational modal analysis of structures*. *Mechanical Systems and Signal Processing, 205*, 111267. https://doi.org/10.1016/j.ymssp.2024.111267
9. Hou, R., & Xia, Y. (2021). *Review on the new development of vibration-based damage identification for civil engineering structures: 2010–2019*. *Journal of Sound and Vibration, 491*, 115741. https://doi.org/10.1016/j.jsv.2020.115741
10. Kiranyaz, S., Avci, O., Abdeljaber, O., Ince, T., Gabbouj, M., & Inman, D. J. (2021). *1D convolutional neural networks and applications: A survey*. *Mechanical Systems and Signal Processing, 151*, 107398. https://doi.org/10.1016/j.ymssp.2020.107398
11. Kita, A., Cavalagli, N., & Ubertini, F. (2019). *Temperature effects on static and dynamic behaviour of Consoli Palace in Gubbio, Italy*. *Mechanical Systems and Signal Processing, 123*, 153–169. https://doi.org/10.1016/j.ymssp.2018.10.021
12. Li, J., Bao, T., & Ventura, C. E. (2021). *An automated operational modal analysis algorithm and its application to concrete dams*. *Mechanical Systems and Signal Processing, 156*, 108707. https://doi.org/10.1016/j.ymssp.2021.108707
13. Liu, Y., Cao, R., Xu, S., & Deng, L. (2023). *A deep learning-based method for structural modal analysis using computer vision*. *Engineering Structures, 285*, 117285. https://doi.org/10.1016/j.engstruct.2023.117285
14. Lucà, F., Manzoni, S., Cigada, A., & Frate, L. (2021). *A vibration-based approach for health monitoring of tie-rods under uncertain environmental conditions*. *Mechanical Systems and Signal Processing, 155*, 108547. https://doi.org/10.1016/j.ymssp.2021.108547

15. Malekloo, A., Ozer, E., & Girolami, M. (2021). *Machine learning and structural health monitoring overview with emerging technology and high-dimensional data source highlights*. *Structural Health Monitoring, 21*(4), 14759217211036880. https://doi.org/10.1177/14759217211036880
16. Park, H. S., & Oh, B. K. (2024). *CNN-based model updating for structures by direct use of dynamic structural response measurements*. *Engineering Structures, 294*, 117880. https://doi.org/10.1016/j.engstruct.2024.117880
17. Santos, A., Figueiredo, E., Silva, M. F. M., Sales, C. S., & Costa, J. C. W. A. (2016). *Machine learning algorithms for damage detection: Kernel-based approaches*. *Journal of Sound and Vibration, 363*, 584–599. https://doi.org/10.1016/j.jsv.2015.11.008
18. Yun, D. Y., Oh, B. K., Park, K., & Park, H. S. (2024). *LSTM-Based Approach for Stable Identification of Modal Damping Ratio in Building Structures*. *Advances in Civil Engineering, 2024*, 6645626. https://doi.org/10.1155/2024/6645626
19. Zhang, Q., Cai, X., Zhong, Y., Tang, X., & Wang, T. (2024). *Dynamic response prediction of high-speed train on cable-stayed bridge based on genetic algorithm and fused neural networks*. *Engineering Structures, 294*, 117869. https://doi.org/10.1016/j.engstruct.2024.117869
20. Zhang, Y., Wang, L., & Xiang, Z. (2012). *Damage detection by mode shape squares extracted from a passing vehicle*. *Journal of Sound and Vibration, 331*(8), 1937–1954. https://doi.org/10.1016/j.jsv.2011.09.004